HAL open science

Detection of Mars Normal Modes From S1222a Event and Seismic Hum

P. Lognonné, M. Schimmel, E. Stutzmann, P. Davis, M. Drilleau, G. Sainton, T. Kawamura, M. P. Panning, W. B. Banerdt

▶ **To cite this version:**

P. Lognonné, M. Schimmel, E. Stutzmann, P. Davis, M. Drilleau, et al.. Detection of Mars Normal Modes From S1222a Event and Seismic Hum. Geophysical Research Letters, 2023, 50, ⟨10.1029/2023GL103205⟩. ⟨insu-04155699⟩

HAL Id: insu-04155699

https://insu.hal.science/insu-04155699v1

Submitted on 7 Jul 2023

HAL is a multi-disciplinary open access archive for the deposit and dissemination of scientific research documents, whether they are published or not. The documents may come from teaching and research institutions in France or abroad, or from public or private research centers.

L'archive ouverte pluridisciplinaire **HAL**, est destinée au dépôt et à la diffusion de documents scientifiques de niveau recherche, publiés ou non, émanant des établissements d'enseignement et de recherche français ou étrangers, des laboratoires publics ou privés.

Distributed under a Creative Commons CC BY-NC-ND 4.0 - Attribution - Non-commercial use - No Derivative Works - International License

Check for updates

ADVANCING EARTH AND SPACE SCIENCE

Geophysical Research Letters

RESEARCH LETTER
10.1029/2023GL103205

Special Section:
The Large Marsquake of Sol 1222

Detection of Mars Normal Modes From S1222a Event and Seismic Hum

P. Lognonné[1], M. Schimmel[2], E. Stutzmann[1], P. Davis[3], M. Drilleau[4], G. Sainton[1], T. Kawamura[1], M. P. Panning[5], and W. B. Banerdt[5]

[1]Université Paris Cité, Institut de physique du globe de Paris, CNRS, Paris, France, [2]Geosciences Barcelona—CSIC, Barcelona, Spain, [3]University of California, Los Angeles, CA, USA, [4]Institut supérieur de l'Aéronautique et de l'Espace, Sup Aéro, Toulouse, France, [5]Jet Propulsion Laboratory, California Institute of Technology, Pasadena, CA, USA

P. Lognonné, M. Schimmel, and E. Stutzmann contributed equally to this work.

Key Points:

- We present the first observational evidence of free oscillations excited by a seismic event and background oscillations on Mars
- We extracted normal modes hidden in low signal-to-noise ratio seismic record using a phasor walkout analysis
- Normal mode frequencies can be used to narrow down published Mars interior models obtained from body wave travel time inversions

Supporting Information:

Supporting Information may be found in the online version of this article.

Correspondence to:

P. Lognonné,
lognonne@ipgp.fr

Citation:

Lognonné, P., Schimmel, M., Stutzmann, E., Davis, P., Drilleau, M., Sainton, G., et al. (2023). Detection of Mars normal modes from S1222a event and seismic hum. *Geophysical Research Letters*, *50*, e2023GL103205. https://doi.org/10.1029/2023GL103205

Received 8 FEB 2023
Accepted 5 MAY 2023

Author Contributions:

Conceptualization: P. Lognonné, M. Schimmel, E. Stutzmann
Data curation: P. Lognonné, E. Stutzmann, T. Kawamura

© 2023. The Authors.
This is an open access article under the terms of the Creative Commons Attribution-NonCommercial-NoDerivs License, which permits use and distribution in any medium, provided the original work is properly cited, the use is non-commercial and no modifications or adaptations are made.

Abstract We present the first detection of normal modes on Mars using the vertical records from InSight's broad-band seismometer following the marsquake that occurred on sol 1222. The proposed catalog lists 60 potential eigenfrequencies between 3 and 12 mHz. Due to their low signal-to-noise ratio, these normal modes were detected using the phasor walkout approach. The normal modes amplitudes are consistent with the upper limit of the S1222a magnitude and with high quality factors. Additionally, we provide the first detection of a Martian hum before the quake for several of these frequencies. The proposed frequencies are at about 1-sigma of those predicted by published models based on body wave travel time inversions. Our detection of normal modes is the first made on a terrestrial planet other than Earth and opens the way for future interior models that incorporate both normal modes frequencies, surface waves velocities and body wave travel times.

Plain Language Summary The frequencies of a planet's global oscillations are closely linked to its internal structure. Thanks to the powerful magnitude 4.7 marsquake that occurred on sol 1222 and to the low long period noise of the very broad band Insight seismometer, we detected 60 normal mode frequencies. Furthermore, we discovered evidence of continuous vibrations on Mars, called Martian hum, as several eigenfrequencies were present before the marsquake occurred. Mars is now the second terrestrial planet after the Earth for which these planetary tones are observed.

1. Introduction

The inversion of normal mode eigenfrequencies is one of the most efficient ways to determine the physically averaged interior structure of a planet, as illustrated by Dziewonski and Anderson (1981), one of the most cited references in seismology. On Earth, normal mode observations require both large quakes, with magnitude larger than 7, and well-shielded, long-period (LP), low-noise seismic instrumentation (Laske & Widmer-Schnidrig, 2015). This delayed the first observation of Earth normal modes until the great $M_w = 9.5$ Chile earthquake in 1960, several decades after the body wave hodochrone table determined by Jeffreys (1937). See Benioff et al. (1961), Lognonné and Clévédé (2002), Laske and Widmer-Schnidrig (2015), among others for reviews of Earth's normal modes.

Despite the challenges presented by the effective deployment of a LP seismometer and the expected lack of very large-magnitude marsquakes, normal mode detection was always an ultimate goal for Mars seismology. This was listed in descriptions of the first Mars seismic exploration projects (Bolt & Derr, 1969; Okal & Anderson, 1978) and remained in most later ones (Gudkova & Zharkov, 1996; Lognonné et al., 1996, 2000; Lognonné & Mosser, 1993) including InSight (Bissig et al., 2018; Lognonné et al., 2019; Lognonné & Johnson, 2015; Panning et al., 2017).

The recording by InSight's (Banerdt et al., 2020) SEIS Very Broad Band (VBB) sensors (Lognonné et al., 2019) of the $M_w \approx 4.7$ S1222a marsquake (InSight Mars Quake Service, 2022; Kawamura et al., 2022) triggered a search for normal modes. Indeed, for the first time, multi-orbiting surface waves have been identified in the time domain (Beghein et al., 2022; Kawamura et al., 2022; Kim et al., 2023; Li et al., 2023; Panning et al., 2023), suggesting the possible presence of normal modes in the frequency domain due to the surface wave-normal mode duality (Dahlen & Tromp, 1998). This event occurred at UTC time 2022-05-04 23:23:07 which corresponds to the Martian Local Mean Solar Time (LMST) sol 1222 03:50:08.9. S1222a marsquake was the first event detected on sol 1222. Therefore it has the label a.

Formal analysis: P. Lognonné, M. Schimmel, E. Stutzmann, P. Davis
Funding acquisition: P. Lognonné, W. B. Banerdt
Investigation: P. Lognonné, W. B. Banerdt
Methodology: P. Lognonné, M. Schimmel, E. Stutzmann
Project Administration: P. Lognonné, M. P. Panning, W. B. Banerdt
Software: P. Lognonné, M. Schimmel, E. Stutzmann, P. Davis, M. Drilleau, G. Sainton
Supervision: P. Lognonné, M. Schimmel, E. Stutzmann
Validation: P. Davis
Visualization: P. Lognonné, M. Schimmel, E. Stutzmann
Writing – original draft: P. Lognonné, M. Schimmel, E. Stutzmann
Writing – review & editing: P. Lognonné, M. Schimmel, E. Stutzmann, P. Davis, M. Drilleau, G. Sainton, T. Kawamura, M. P. Panning, W. B. Banerdt

The S1222a marsquake is, however, a low magnitude quake for exciting normal modes. Lognonné et al. (1996, 2005) estimated the ∼5 mHz normal mode amplitude excited by a 10^{18} Nm Marsquake at 90° epicentral distance to be about 10^{-8} m/s^2/Hz$^{1/2}$ for 1 day spectra. Rescaling gives, for the estimated seismic moment of S1222a ($0.7 - 2.6 \times 10^{16}$Nm) and at 37° of epicentral distance, an amplitude below 3.5×10^{-10} m/s^2/Hz$^{1/2}$, which is close to the lowest noise observed by SEIS (Lognonné et al., 2020; Stutzmann et al., 2021). In addition, S1222a occurred slightly before 04:00 LMST (Kawamura et al., 2022). Thus, the first 12 hr after this event correspond to daytime, during which the environmental noise is the largest (Lognonné et al., 2020).

In this study, we perform a careful analysis of the two outputs of the VBB seismometer signals (InSight Mars SEIS Data Service, 2019). These two outputs, the POS long period channel and the VEL broadband channel, are sensitive to the same accelerometric signal, but with a different transfer function and more importantly, with different and non-coherent self noises. See more in Lognonné et al. (2019).

We first show that normal mode search based on spectra analysis alone cannot provide meaningful normal mode identification, due to the low signal-to-noise ratio. As an alternative, we use a phasor walkout analysis and identify a set of 60 frequencies for which the phasor walkout is structured in the 3–12 mHz bandwidth. These stable oscillatory patterns are interpreted as Martian normal modes. Most of them can be associated with fundamental modes, and in several cases, the proximity of frequencies is consistent with possible splitting effects.

Despite their challenging low amplitude, normal modes are therefore detected for the first time on a terrestrial planet other than the Earth. We show furthermore that some of these modes are not only excited by S1222a, but were also present in the noise prior to this marsquake. This is the first observational evidence of a Martian hum, predicted as a consequence of the Martian atmospheric circulation and boundary layer activity (Kobayashi & Nishida, 1998; Lognonné & Johnson, 2015; Nishikawa et al., 2019).

We finally show that these possible normal mode frequencies reasonably match the spheroidal fundamental normal modes computed for published Mars interior models derived from body waves analysis. This provides an additional validation of our proposed frequency collection and confirms the very high potential of phasor walkout analysis for future analysis on the full InSight SEIS data set, including new Mars interior models derived from joint inversions of body waves, surface waves and normal modes.

2. Data Processing and Approach

Due to the soft ground and harsh environmental conditions on Mars, different aseismic signals are recorded together with seismic waves (Ceylan et al., 2021; Lognonné et al., 2020; Scholz et al., 2020; Stutzmann et al., 2021). By far the highest-amplitude aseismic signals are glitches, mostly caused by the response of the seismometer and its materials to the severe temperature variations. Glitch amplitudes can be a few orders of magnitude larger than the recorded seismic waves. Glitches affect both low-frequency waveforms and amplitude spectra, and cannot be removed by frequency filtering. Moreover, many glitches occur during the cooling of the SEIS hardware and Mars ground after sunset. Glitch removal is difficult and different strategies exist (Lognonné et al., 2020; Scholz et al., 2020) to provide glitch-reduced datasets.

Here, an additional effort to remove glitches was performed on the 2 sps data following Lognonné et al. (2020) to obtain the cleanest possible data set at long periods. Glitches identified on the VEL channel have also been removed from the POS channel. Figure S1 in Supporting Information S1 shows the lowest noise spectra obtained from raw data and from deglitched data with different deglitching threshold values. These spectra are computed using 12 hr of data between 14:00 LMST on sol 1222 and 02:00 LMST on sol 1223. Crustal Rayleigh waves, with group velocity of 2.88 km/s (Panning et al., 2023), will orbit about 6 times while 200 s mantle waves will orbit about 8 times due to larger group velocity of 3.90 km/s (Figure S2 in Supporting Information S1). Figure S1 in Supporting Information S1 shows that deglitching is necessary and reduces the noise by a factor of 10. This also shows the low amplitude of deglitched spectra, with peak amplitudes for frequencies below 5 mHz smaller than four times the expected electronics self-noise spectral mean amplitude of the VBB (about 2×10^{-9} m/s^2/Hz$^{1/2}$ for the VEL channel and 1.2×10^{-9} m/s^2/Hz$^{1/2}$ for the POS channel at 5 mHz, which leads typically to peak spectral amplitude up to about 2.5 these mean values).

At such low amplitudes, further data complexity is revealed in the slight differences between POS and VEL. Figure S3 in Supporting Information S1 shows the coherence and amplitude ratio between POS and VEL

19448007, 2023, 12, Downloaded from https://agupubs.onlinelibrary.wiley.com/doi/10.1029/2023GL103205 by Cochrane France, Wiley Online Library on [07/07/2023]. See the Terms and Conditions (https://onlinelibrary.wiley.com/terms-and-conditions) on Wiley Online Library for rules of use; OA articles are governed by the applicable Creative Commons License

deglitched data. Below 20 mHz bandwidth during the lowest noise time-period (after 18 hr LMST), the coherency drop confirms the larger self-noise for VEL than for POS, as predicted by instrument performances (Lognonné et al., 2019). At lower frequencies, intermittent coherency drops correspond to larger POS noise, related to small electronic glitches specific to the POS channel that were not removed during the data deglitching process.

Glitches or other artifacts therefore remain in the data and require further special care to avoid any bias and possible misinterpretations of the results. This is particularly the case for spectral amplitudes analysis. In the latter, free oscillations are expected to generate peaks in power or amplitude spectra. In addition to classical methods, we tested other spectral autocorrelation estimations: the multi-taper approach in Park and Lindberg (1987), which relies on a sequence of several prolate spheroidal tapers to minimize spectral leakage, and the phase cross-correlation approach (Schimmel, 1999). This technique has proven to be robust against outlying amplitude signals (Schimmel et al., 2018).

As shown in the next section, none of these techniques provided evidence of normal mode peaks. We therefore conducted a phasor walkout analysis (Schimmel et al., 2002; Zurn & Rydelek, 1994), which was successful. In the following we briefly introduce each method, and we show the failure of spectral amplitude methods and the success of phasor walkout analysis, which was then employed to create the first preliminary normal mode catalog for Mars.

2.1. Phase Correlation and Multi-Taper Spectra

Generally, detection of normal modes and measurement of their frequencies rely on the estimation of the power or energy spectral density (PSD or ESD) computed with the Fourier Transform of differently defined autocorrelation functions. PSD is employed for infinite signal energy, which inhibits a direct application of the Fourier transform. Conversely, the ESD can be computed for transient waveforms and equals the squared amplitude spectrum of the seismic recording. In any case, the differently defined autocorrelations measure self-similarity, that is, the similarity of a time-series with a delayed version of itself to obtain the spectral contents.

In Schimmel et al. (2018), the conventional autocorrelation functions have been replaced by the phase autocorrelation (hereafter PCC, for phase cross-correlation) (Schimmel, 1999) to show that this procedure achieves robust spectra for mode detection. Among the main advantages are that phase cross-correlations are amplitude unbiased as they are based on envelope normalized analytic signals, and that they measure signal similarity by the total time of phase coherence rather than the product of amplitudes. It is thus an independent approach that does not measure the frequency-dependent variance distribution in the data. Therefore, phase correlation is very robust to strong outlying signals such as glitches (see Schimmel et al. (2018) for comparisons and examples).

To search for modes we use 128,000 s long (≃35 hr) S1222a event recordings from the vertical POS and VEL channels. Records start at Marsquake Service (MQS) event origin time (23:23:07 UTC on day 124 of the year 2022) (Kawamura et al., 2022). Here we focus on modes between 3 and 12 mHz and decimated the data to a sample interval of 2 s after frequency band-passed filtering between 2.5 and 12.5 mHz. PCC lag-time window is 100,000 s (≃28 hr), corresponding to 18.3 orbits for 200 s surface wave.

Finally, the spectral estimation of the PCC is performed with multi-tapers (Park & Lindberg, 1987). This method employs a small set of orthogonal data tapers rather than one single taper to weight the data and to finally construct a high-resolution power spectrum with minimum spectral leakage.

Figure 1 shows the spectral representation of the deglitched recordings from the vertical POS and VEL channels. The deglitching threshold is 24% and the spectra were computed using the multi-taper and PCC approach. Several maxima in the spectra are observed. Although the POS (blue line) and VEL (red line) spectra look different, we observe that most of the time, both spectra contain maxima at the same frequencies. Due to the low signal level, the common signal in POS and VEL channels is affected differently by the instrument noise. For VEL and POS, this noise is related to the integrator of the VBB feedback, and the displacement transducer, respectivelly (Lognonné et al., 2019).

The coincidence of maxima in the presence of different self-noise does not guarantee that these maxima are normal modes, as those can also be generated by common seismic noise. We therefore consider each spectral maximum as a potential mode signal and we then search in their phase for a potential normal mode signature with the phasor walkout method (Schimmel et al., 2002; Zurn & Rydelek, 1994). Note that low amplitude maxima are not located at the center of the spectral peak. We therefore also analyze frequencies at the center of each peak.

19448007, 2023, 12, Downloaded from https://agupubs.onlinelibrary.wiley.com/doi/10.1029/2023GL103205 by Cochrane France, Wiley Online Library on [07/07/2023]. See the Terms and Conditions (https://onlinelibrary.wiley.com/terms-and-conditions) on Wiley Online Library for rules of use; OA articles are governed by the applicable Creative Commons License

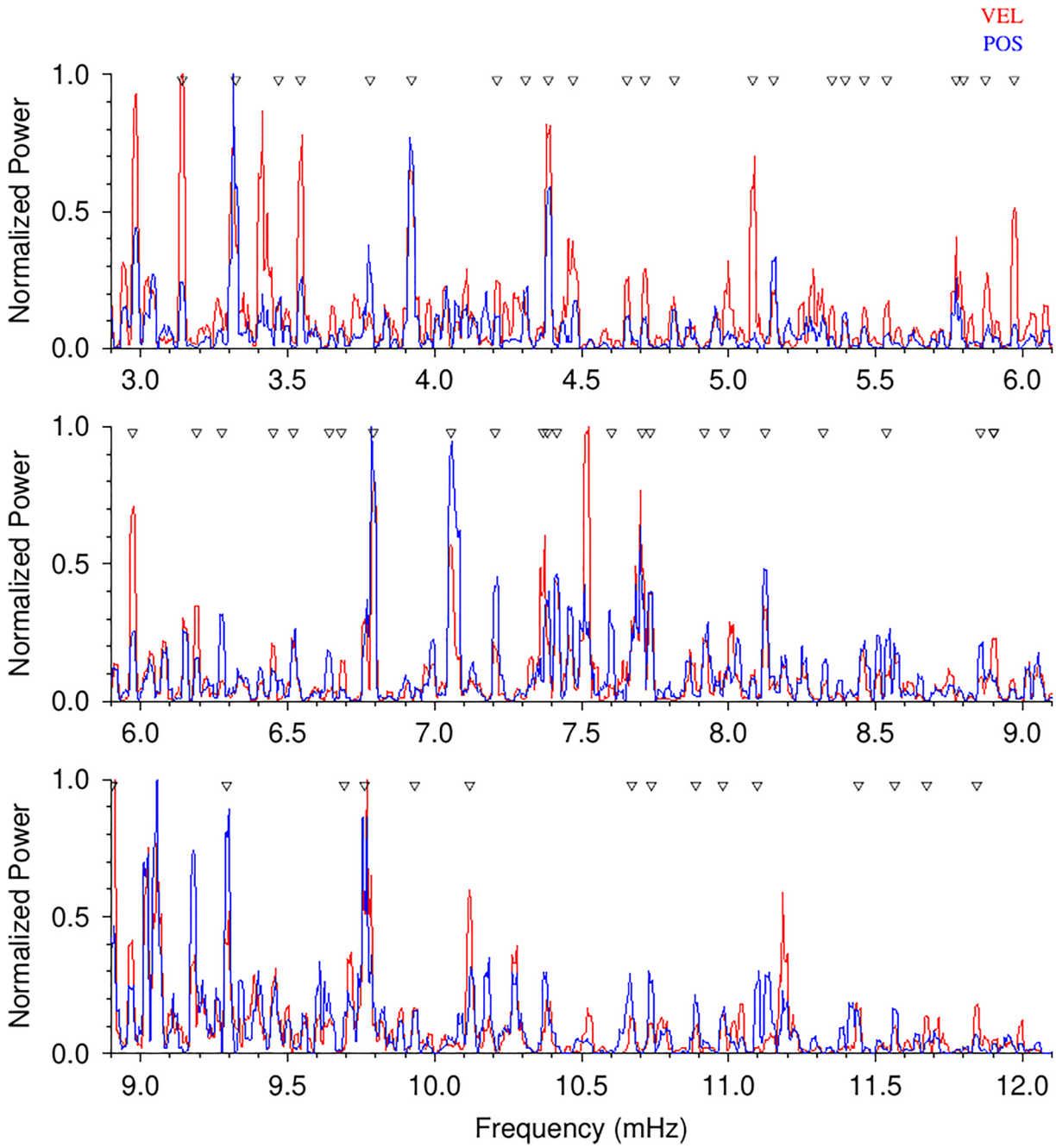

Figure 1. Phase autocorrelation spectra. Spectral representation of the POS and VEL channel deglitched data for the vertical component. The deglitching (Lognonné et al., 2020; Scholz et al., 2020) was made with a threshold of 24%. Spectra have been computed using the multi-taper approach on phase auto-correlation. Amplitudes have been normalized for visualization purposes. The inverted triangles mark frequencies with straight phasor walkout segments.

2.2. Phasor Walkouts

The phasor-walkout approach visualizes the construction of a Fourier amplitude spectrum at a fixed frequency as a vector summation in the complex number space. It is the graphical representation of the Fourier transform, which permits to track the spectral summation as function of time. See Zurn and Rydelek (1994) for a review and further references and Majstorović et al. (2018) for recent application to normal mode search. A synthetic example can be seen in Figure S4 in Supporting Information S1, for a signal with an harmonics 5.1 mHz oscillation, with a duration of 20,000 s and a quality factor Q of 200. This illustrates the differences of phasor walkouts between frequencies where the amplitudes are dominated by the signal and those contaminated by noise.

19448007, 2023, 12, Downloaded from https://agupubs.onlinelibrary.wiley.com/doi/10.1029/2023GL103205 by Cochrane France, Wiley Online Library on [07/07/2023]. See the Terms and Conditions (https://onlinelibrary.wiley.com/terms-and-conditions) on Wiley Online Library for rules of use; OA articles are governed by the applicable Creative Commons License

Thus, the inspection of the phasor walkout assesses how the spectral amplitude has been built up and consequently distinguishes between fortuitous random summation and long-duration small amplitude oscillations. Straight walkout matters more than the absolute amplitude, that is, straight walkouts of small amplitude oscillations should not be penalized as they might be due to a small-energy mode.

Phasor walkouts are in analogy to Fourier theory subject to outlying amplitude signals. Although the data have been carefully deglitched, some glitches and other artifacts are still likely present. We therefore compute the phasor walkouts for time-domain autocorrelations obtained with PCC. PCC is amplitude unbiased (Schimmel et al., 2018) and time-domain autocorrelations are related to spectral density. The time evolution of the walkout is then, however, related to the autocorrelation lag-time.

We made our search on all peaks of the two POS-Z and VEL-Z spectra, whatever their amplitudes were (Figure 1). For all peaks, we consider the frequency at the maximum amplitude and at its centroid. Phasor walkouts are computed for all these frequencies and the selection of the mode frequencies is described in the next section.

2.3. Mode Catalog

We visually inspected all phasor walkouts and selected those that are the straightest for several hours. In some clear cases, we accepted a walkout interruption by some other noise before the straight walkout continuation in the same direction. Several examples of walkouts are illustrated in Figure 2. The start time of the trace is at 1,000 s lag time and the color changes every 3 hours to provide a notion of time. We select the frequencies with straight phasor from both vertical POS and VEL channels, and merged them to obtain a single catalog. In some cases, a straight walkout is seen on both channels simultaneously, while at other frequencies only one of the two channels produces a straight walkout. Both channels are independent as containing different instrumental noise. It is therefore not a surprise that some of the weak amplitude modes are only seen on one of the channels. Finally, we obtain 60 frequency measurements presented in our mode catalog (Table S1 and Figures S5–S10 in Supporting Information S1 for all phasor walks of these normal modes candidates), which we attribute to harmonic oscillations. These frequencies have also been marked as inverted triangles in Figure 1. Note the presence of a few clusters of 2–3 close frequencies which might be related to split normal modes and therefore to a single fundamental multiplet.

2.4. Martian Background Oscillations

We further inspected phasor walkouts before and after the S1222a event using the mode frequencies from Table S1 in Supporting Information S1. Surprisingly, linear walkouts can be identified before the event for some of the frequencies (Figure 3) on both the POS and VEL output. It is observed that a few straight walkout segments change direction close to origin time (Figures 3a, 3b, 3d, and 3f). These oscillations were therefore present in the signal before the S1222a event. If associated with normal modes, these are Martian background oscillations as no other large events happened on Mars the few sols before S1222a event (Clinton et al., 2020; InSight Mars Quake Service, 2022).

Normal modes are expected indeed to be excited by the Martian atmosphere (Kobayashi & Nishida, 1998; Tanimoto et al., 1998). This correspond to the Hum on Earth, whose sources, however, are mostly in the oceans (Ardhuin et al., 2015). Nishikawa et al. (2019) consider the global atmospheric circulation as an Hum source and estimate its strength to be comparable to a 4.9 magnitude marsquake, with a better excitation efficiency in the 2–5 mHz bandwidth. This magnitude is close to the magnitude 4.7 proposed for S1222a and consistent with our observations.

Despite the different excitation on Earth and Mars, we use the expression Martian Hum (MHum) to refer to the background oscillations on Mars. The observed change of the phasor direction for some frequencies can be explained by a phase change owing to an external source and/or a variation of the central frequency for multiplets due to differences in singlet's excitations.

The strength of the MHum depends on both the atmospheric sources and of the strength of atmospheric coupling. As shown by Lognonné and Johnson (2015), the strength of atmospheric coupling is modulated at long period by resonances with the atmosphere found with about a 1.1 mHz spacing and with up to a factor 5 of differences between the maxima and minima of coupling. Therefore, the MHum is most likely not exciting the normal modes

19448007, 2023, 12, Downloaded from https://agupubs.onlinelibrary.wiley.com/doi/10.1029/2023GL103205 by Cochrane France, Wiley Online Library on [07/07/2023]. See the Terms and Conditions (https://onlinelibrary.wiley.com/terms-and-conditions) on Wiley Online Library for rules of use; OA articles are governed by the applicable Creative Commons License

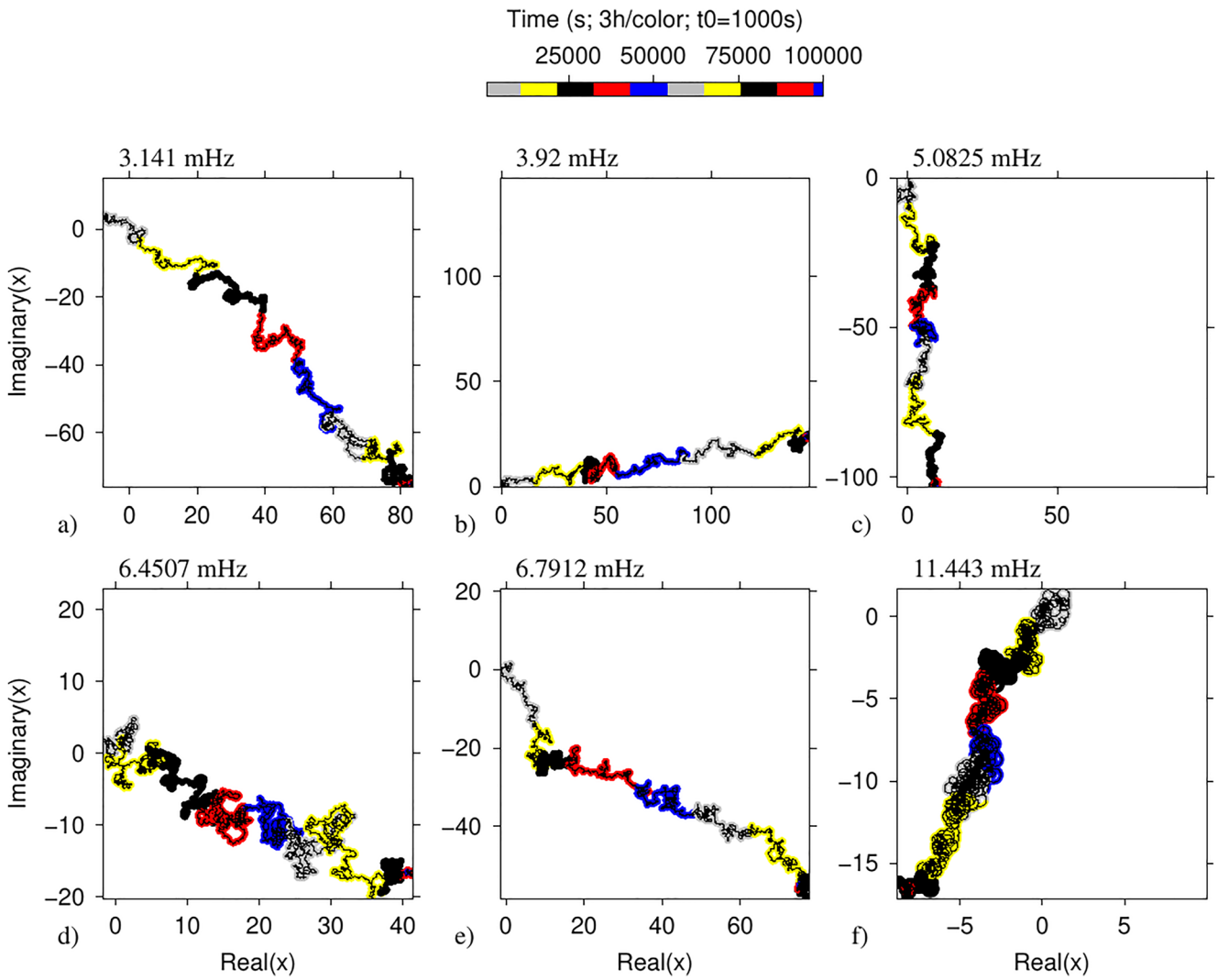

Figure 2. Phasor walkout examples for six different frequencies. The underlying data are time-domain phase auto-correlation computed for S1222a recordings from the vertical VEL (a, c, d, and f) and POS (b and e) channels. Lag time window is from 1,000 to 100,000 s and color changes every 3 hr. The PWOs shown in (d and f) are more noisy, but still indicate straight walkouts as function of time as seen by the color sequence.

in the same way, which might be a first explanation for the non-systematic presence of MHum at the Mars normal modes frequencies excited by S1222a. More analysis is planned with the full VBB data set to confirm these first observations.

3. Discussion of Observations and Conclusion

Normal modes are expected to have small amplitudes (Lognonné, 2005; Lognonné et al., 1996) and their detection might appear surprising. Several findings from SEIS are, however, supporting larger normal mode signals as compared to pre-launch expectations. The first are the event mechanisms. While thermo-elastic cooling events were baselined prior to launch, marsquake mechanisms of normal or reverse faulting, and even strike-slip have been proposed (Brinkman et al., 2021; Jacob et al., 2022; Sita & van der Lee, 2022) which generate much larger amplitudes, especially at low frequency. The mantle intrinsic attenuation is also lower (Giardini et al., 2020; Lognonné et al., 2020) than pre-launch estimates (Smrekar et al., 2019). Low attenuation is expected in the thermal lithosphere and therefore in the first 400–500 km, where the detected normal modes have most of their energy. Figure S11 in Supporting Information S1 shows spectra of 36 hr of synthetics with the first 20 spheroidal modes branches computed with the TAYAK pre-launch model with regolith (Smrekar et al., 2019) and the upper

19448007, 2023, 12, Downloaded from https://agupubs.onlinelibrary.wiley.com/doi/10.1029/2023GL103205 by Cochrane France, Wiley Online Library on [07/07/2023]. See the Terms and Conditions (https://onlinelibrary.wiley.com/terms-and-conditions) on Wiley Online Library for rules of use; OA articles are governed by the applicable Creative Commons License

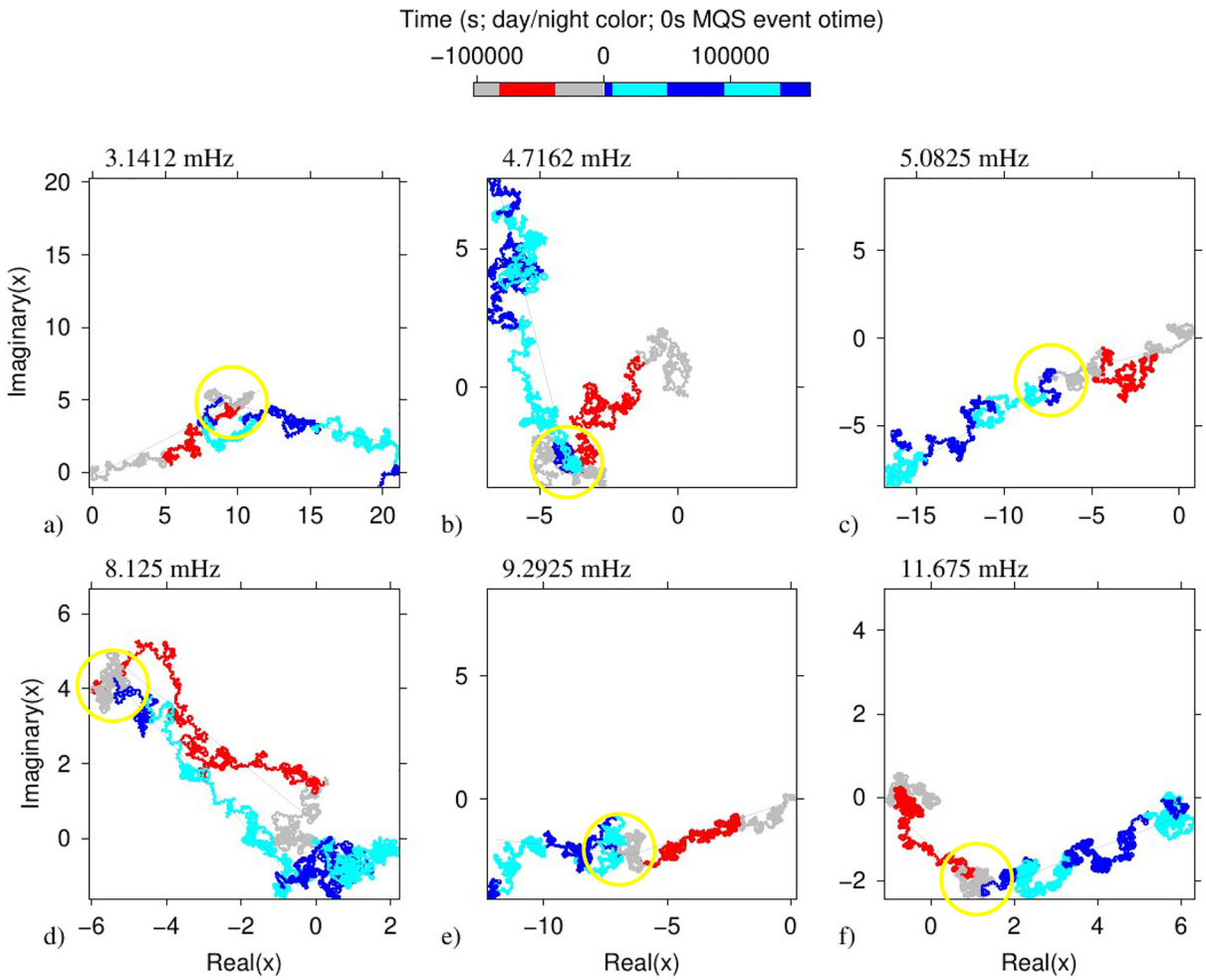

Figure 3. Phasor walkout examples. Shown are six walkouts with straight segments before and after the S1222a event. Underlying data are VEL recordings and 0 s is at event origin time. Red/gray colors mark day/night time before the event while blue/cyan mark the night/day time after the event. Most striking is the change in direction of the linear walkouts after occurrence of the event, marked by the yellow circles, at some of the frequencies (a, b, d, and f). Straight black lines approximate the straight walkout.

value of MQS moment (2.6 10^{16} Nm). As for our data analysis, we get a low SNR compared to the VBB self noise. These synthetics show a signal dominated by the fundamental Rayleigh modes. Although the SNR with respect to the POS output is smaller than 3, the normal mode signature is comparable to what was observed on the data spectra, which suggests that the quality factor Q is larger than 300. For this low signal-to-noise condition, the phasor walkout approach, which visualizes the build up of a spectral amplitude, is crucial to distinguish fortuitous spectral summation of noise from weak amplitude oscillations ringing for several hours. Our observations are therefore compatible with estimations from spherically symmetric modeling. Additional work, including lateral variations models and frequency-dependent attenuation, is required for a complete understanding of the observed amplitudes of the normal modes candidates and for the estimation of Qs.

Our preliminary mode catalog, based on phasor walkout inspections, is therefore compatible with the modeled strength of Rayleigh normal mode signal for both S1222a and MHum. In the 3–12 mHz bandwidth where our 60 frequencies were found, we expect about 50 Rayleigh modes. Several frequencies are closer than the typical spacing between these modes, which could be due to splitting. Although we cannot exclude a few spheroidal overtones or even toroidal modes with vertical amplitude, as on Earth (Masters et al., 1983), we focus now only on Rayleigh fundamental modes.

For most frequencies, the seismic origin is supported by the parallel POS and VEL phasor walkouts (Table S2 in Supporting Information S1). We nevertheless cannot exclude some periodic noise despite deglitching (Barkaoui

19448007, 2023, 12, Downloaded from https://agupubs.onlinelibrary.wiley.com/doi/10.1029/2023GL103205 by Cochrane France, Wiley Online Library on [07/07/2023]. See the Terms and Conditions (https://onlinelibrary.wiley.com/terms-and-conditions) on Wiley Online Library for rules of use; OA articles are governed by the applicable Creative Commons License

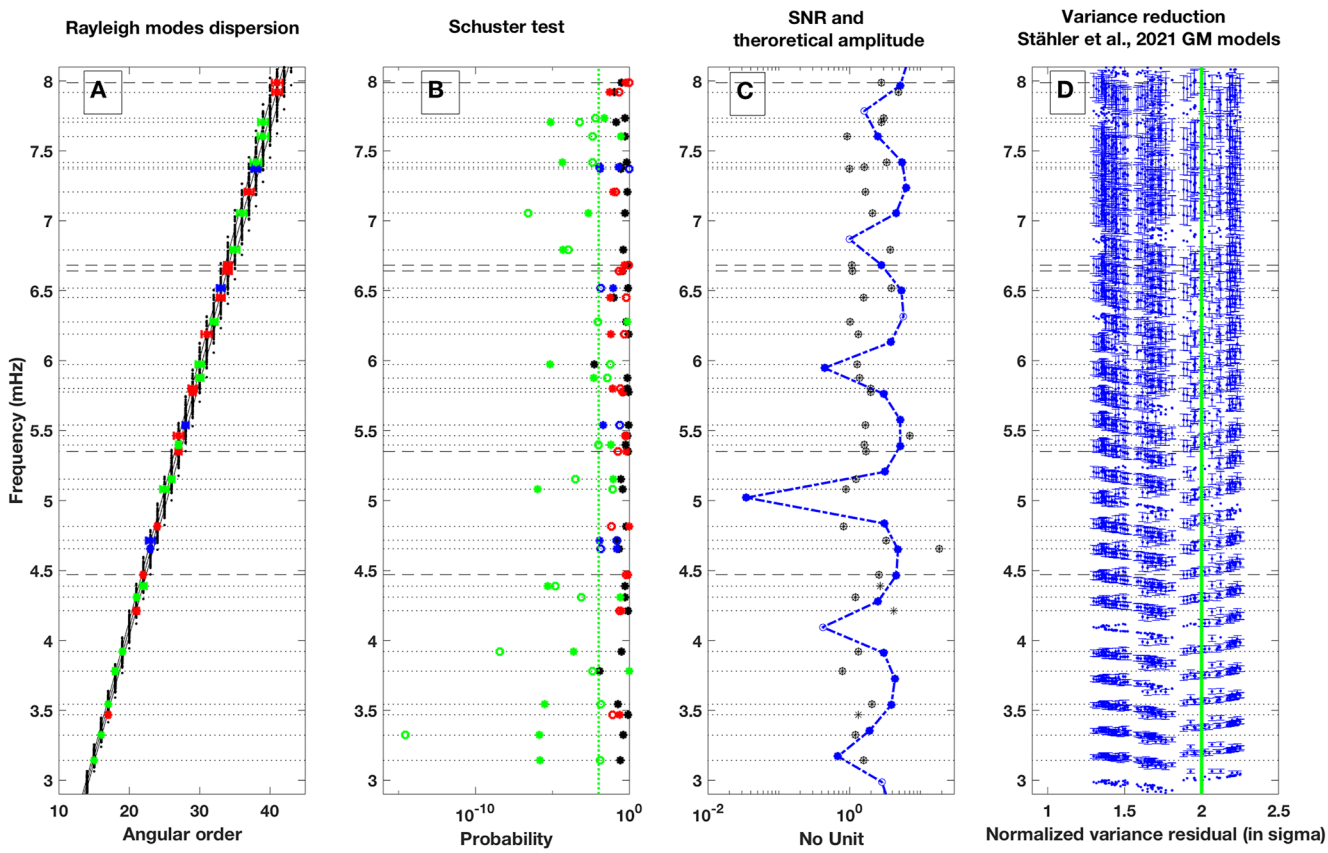

Figure 4. Fit between observed frequencies (horizontal lines) and those computed for the 100 geodynamical models proposed in Stähler et al. (2021). For all figures, vertical axis is the frequency in mHz, the identified frequencies are shown in dotted and long dashed lines. For (a and b), Schuster test probability is shown with the following color code: green, for the best when either the POS or VEL walkout is below 1%. Blue when the best is between 1% and 5%. Red when both are above 5%. From left to right (a) the spheroidal fundamental modes as a function of their angular order. For each model, normal mode frequencies are shown by black dots. The estimated angular order of the modes is shown with a color dot corresponding to the Schuster test and with the posteriori angular order variance. (b) Schuster test value for all modes, shown with empty circle for VEL and filled circle for POS, with color codes listed above. The green vertical line recalls the 99% threshold for quality (a). The black filled circles provide the Schuster test for the difference between POS and VEL, which is a proxy for sensor noise. When the value for this difference is smaller than the one obtained for the POS or VEL channels, this reduces the confidence on the detected mode due to possible sensor origin. Such case is found for frequencies shown with long dashed lines at about 4.47, 5.35, 6.64, 6.68, and 7.99 mHz. (c) Comparison between the observed amplitude SNR of the spectral peaks (defined as the square root of the ratio between the absolute value of the difference between POS and VEL power and the POS and VEL mean power value) with stable phasor walkout (gray symbols) and the variation of the modified Legendre function $P_\ell^1(\theta)$, where θ is the epicentral distance of S1222a, taken as 37° (Kawamura et al., 2022). For a normal or reverse fault, $P_\ell^1(\theta)$ dominates the amplitude as compared to $P_\ell^0(\theta)$ or $P_\ell^2(\theta)$. Note that SNR for all modes are ranging from 1 to 3 which is in accordance with expected amplitudes. Filled blue circles are the frequencies for the best fitted GM models of Stähler et al. (2021), while empty blue circles mark frequencies for which no stable phasor peak is found within less than 1/3 of the distance between two consecutive mode frequencies. Two out of the three missing frequencies (close to 4 and 5 mHz) correspond to nodes of $P_\ell^1(\theta)$, and are therefore possible node of the S1222a spectra. (d) Misfit between observed frequencies and all modes for all models. Accepted modes are shown with the associated splitting frequency error bar, while the rejected ones are just marked with a blue dot. The best models have an average misfit variance of about 1.3 σ, with penalty term in panel (d) and 0.8 σ without penalty term (Figure S14 in Supporting information S1). The green vertical line provides the average best misfit obtained when the 60 frequencies in the 3–12 mHz bandwidth are replaced by random frequencies.

et al., 2021; Kim et al., 2021) or even random origin for a few frequencies. We therefore performed Schuster tests (See details in supplementary Section 3 in Supporting Information S1), already used for phasor-walk analysis (Heaton, 1982; Zurn & Rydelek, 1994), which provide confidence levels for all observed frequencies (Table S3 in Supporting Information S1 and Figure 4b). With these criteria and in the 3–8 mHz bandwidth, where we identified 40 modes and might have about 27 fundamental modes, 19 have confidence above 99% and 6 between 95% and 99%.

The last validation is to test our collection with the theoretical normal mode frequencies from existing mantle models derived from body-wave inversions (Drilleau et al., 2022; Durán et al., 2022; Khan et al., 2022; Stähler et al., 2021). All these models are compared in Lognonné et al. (2023). We follow Panning et al. (2017), where the model misfit is only controlled by the misfit between observed and computed frequencies. This misfit, however,

19448007, 2023, 12, Downloaded from https://agupubs.onlinelibrary.wiley.com/doi/10.1029/2023GL103205 by Cochrane France, Wiley Online Library on [07/07/2023]. See the Terms and Conditions (https://onlinelibrary.wiley.com/terms-and-conditions) on Wiley Online Library for rules of use; OA articles are governed by the applicable Creative Commons License

can be affected by the frequency shifts associated with lateral variations within Mars, in ways similar to what is observed on Earth (Lognonné & Clévédé, 2002). We therefore consider a splitting dispersion, introduced here as observation error of the observed frequencies, assumed to be 0.45% at 3 mHz, with a linear trend leading to 1.1% at 8 mHz. For comparison, Li et al. (2023) propose at about 25 mHz a difference of 1.7% between the averaged group velocity of R1 and the one of R2 for S1222a.

Figure S12 in Supporting Information S1 shows, for the ≃1,500 models collection of Stähler et al. (2021), Khan et al. (2022), Durán et al. (2022), and Drilleau et al. (2022), a misfit of the fundamental spheroidal mode frequencies ranging from slightly more than 1-σ to about 2.5-σ in the 3–8 mHz frequency band. Figure 4d illustrates the misfits for the 100 geodynamical models from Stähler et al. (2021), compared to those obtained from random frequencies collection. Interestingly, the frequency gaps for which no stable frequency were found, around 4 and 5 mHz, are predicted by theoretical amplitudes of normal modes when the excitation of the modified Legendre function $P_\ell^1(\theta)$ is predominant, θ being the estimated 37° epicentral distance (Figure 4c). This is achieved for low dip or when the rake is closed from 90° (Aki & Richards, 2002; Lognonné & Clévédé, 2002), a case already observed for several marsquakes associated with an invert fault mechanism (Brinkman et al., 2021; Jacob et al., 2022; Sita & van der Lee, 2022). This comparison with models allows also to propose preliminary angular orders for these frequencies. This is achieved by computing the probability of these angular orders. This confirms the presence of clusters all associated with the same multiplet (see discussion in Supporting Information S1). Proposed angular orders are provided in Table S1 in Supporting Information S1 and Figure 4a.

In conclusion, despite the low signal-to-noise ratio for frequencies below 12 mHz, we propose a first list of 60 frequencies in the bandwidth 3–12 mHz which includes a large fraction of spheroidal fundamental modes and likely most of them in the 3–8 mHz bandwidth. More work is however necessary for fully characterizing these modes, in term of angular order and presence of overtones. The detection of these normal modes suggest smaller attenuation than InSight pre-launch estimates. Furthermore, a subset of these normal modes candidates were excited, with different excitation coefficients in phase, prior to the S1222a event, which is compatible with a Martian Hum with a strength comparable to S1222a. While further work is needed to fully confirm and characterize these normal modes candidates, Mars might now be considered as the second terrestrial planet after Earth for which normal modes have been detected.

Data Availability Statement

All raw waveform data is available through the InSight Mars SEIS Data Service at IPGP, IRIS-DMC, and NASA PDS (InSight Mars SEIS Data Service, 2019).

Acknowledgments
We acknowledge NASA, CNES, their partner agencies and Institutions (UKSA, SSO, DLR, JPL, IPGP-CNRS, ETHZ, IC, MPS-MPG) and the flight operations team at JPL, SISMOC, MSDS, IRIS-DMC and PDS for providing SEED SEIS data. We thank reviewers for constructive comments. French co-authors acknowledge the French Space Agency CNES and ANR (ANR-19-CE31-0008). PL, ES, TK, GS acknowledge Idex Paris Cité (ANR-18-IDEX-0001). M.P.P. and W.B.B were supported by the NASA InSight mission and funds from the Jet Propulsion Laboratory, California Institute of Technology, under a contract with the National Aeronautics and Space Administration (80NM0018D0004). This is InSight contribution ICN 284.

References

Aki, K., & Richards, P. G. (2002). *Quantitative seismology* (2nd ed.). University Science Books.

Ardhuin, F., Gualtieri, L., & Stutzmann, E. (2015). How ocean waves rock the Earth: Two mechanisms explain microseisms with periods 3 to 300 s. *Geophysical Research Letters*, *42*(3), 765–772. https://doi.org/10.1002/2014gl062782

Banerdt, W. B., Smrekar, S. E., Banfield, D., Giardini, D., Golombek, M., Johnson, C. L., et al. (2020). Initial results from the insight mission on Mars. *Nature Geoscience*, *13*(3), 183–189. https://doi.org/10.1038/s41561-020-0544-y

Barkaoui, S., Lognonné, P., Kawamura, T., Stutzmann, l., Seydoux, L., de Hoop, M. V., et al. (2021). Anatomy of continuous Mars SEIS and pressure data from unsupervised learning. *Bulletin of the Seismological Society of America*, *111*(6), 2964–2981. https://doi.org/10.1785/0120210095

Beghein, C., Li, J., Weidner, E., Maguire, R., Wookey, J., Lekić, V., et al. (2022). Crustal anisotropy in the martian lowlands from surface waves. *Geophysical Research Letters*, *49*(24), e2022GL101508. https://doi.org/10.1029/2022GL101508

Benioff, H., Press, F., & Smith, S. (1961). Excitation of the free oscillations of the Earth by earthquakes. *Journal of Geophysical Research*, *66*(2), 605–619. https://doi.org/10.1029/JZ066i002p00605

Bissig, F., Khan, A., van Driel, M., Stähler, S. C., Giardini, D., Panning, M., et al. (2018). On the detectability and use of normal modes for determining interior structure of Mars. *Space Science Reviews*, *214*(8), 1–28. https://doi.org/10.1007/s11214-018-0547-9

Bolt, B. A., & Derr, J. S. (1969). Free bodily vibrations of the terrestrial planets. *Vistas in Astronomy*, *11*, 69–102. https://doi.org/10.1016/0083-6656(69)90005-1

Brinkman, N., Stähler, S., Giardini, D., Schmelzbach, C., Khan, A., Jacob, A., et al. (2021). First focal mechanisms of marsquakes. *Journal of Geophysical Research: Planets*, *126*(4), e2020JE006546. https://doi.org/10.1029/2020JE006546

Ceylan, S., Clinton, J., Giardini, D., Bose, M., Charalambous, C., Driel, M. v., et al. (2021). Companion guide to the marsquake catalog from insight, sols 0-478: Data content and non-seismic events. *Physics of the Earth and Planetary Interiors*, *310*, 106597. https://doi.org/10.1016/j.pepi.2020.106597

Clinton, J. F., Ceylan, S., van Driel, M., Giardini, D., Stähler, S. C., Böse, M., et al. (2020). The Marsquake catalog from InSight sols 0–478. *Physics of the Earth and Planetary Interiors*, *310*, 106595. https://doi.org/10.1016/j.pepi.2020.106595

Dahlen, F., & Tromp, J. (1998). *Theoretical global seismology*. Princeton University Press.

Drilleau, M., Samuel, H., Garcia, R. F., Rivoldini, A., Perrin, C., Michaut, C., et al. (2022). Marsquake locations and 1-d seismic models for Mars from insight data. *Journal of Geophysical Research: Planets*, *127*(9), e2021JE007067. https://doi.org/10.1029/2021JE007067

19448007, 2023, 12, Downloaded from https://agupubs.onlinelibrary.wiley.com/doi/10.1029/2023GL103205 by Cochrane France, Wiley Online Library on [07/07/2023]. See the Terms and Conditions (https://onlinelibrary.wiley.com/terms-and-conditions) on Wiley Online Library for rules of use; OA articles are governed by the applicable Creative Commons License

Durán, C., Khan, A., Ceylan, S., Charalambous, C., Kim, D., Drilleau, M., et al. (2022). Observation of a core-diffracted P-wave from a farside impact with implications for the lower-mantle structure of Mars. *Geophysical Research Letters*, *49*(21), e2022GL100887. https://doi.org/10.1029/2022GL100887

Dziewonski, A. M., & Anderson, D. L. (1981). Preliminary reference Earth model. *Physics of the Earth and Planetary Interiors*, *25*(4), 297–356. https://doi.org/10.1016/0031-9201(81)90046-7

Giardini, D., Lognonné, P., Banerdt, W. B., Christensen, U., Clinton, J., van Driel, M., et al. (2020). The seismicity of Mars. *Nature Geoscience*, *13*(3), 205–212. https://doi.org/10.1038/s41561-020-0539-8

Gudkova, T., & Zharkov, V. (1996). The exploration of Martian interiors using the spheroidal oscillation method. *Planetary and Space Science*, *44*(11), 1223–1230. https://doi.org/10.1016/S0032-0633(96)00124-9

Heaton, T. H. (1982). Tidal triggering of earthquakes. *Bulletin of the Seismological Society of America*, *72*(6A), 2181–2200. https://doi.org/10.1785/bssa07206a2181

InSight Mars Quake Service. (2022). *Mars seismic catalogue v12, insight mission*. ETHZ, IPGP, JPL, ICL, University of Bristol. https://doi.org/10.12686/a18

InSight Mars SEIS Data Service. (2019). *Seis raw data, insight mission*.IPGP, JPL, CNES, ETHZ, ICL, MPS, ISAE-Supaero, LPG, MFSC. https://doi.org/10.18715/SEIS.INSIGHT.XB_2016

Jacob, A., Plasman, M., Perrin, C., Fuji, N., Lognonné, P., Xu, Z., et al. (2022). Seismic sources of InSight marsquakes and seismotectonic context of Elysium Planitia, Mars. *Tectonophysics*, *837*, 229434. https://doi.org/10.1016/j.tecto.2022.229434

Jeffreys, H. (1937). The density distributions in the inner planets. *Geophys. Suppl. to the Monthly Notices of the Roy. Astr. Soc.*, *4*(1), 62–71. https://doi.org/10.1111/j.1365-246X.1937.tb00410.x

Kawamura, T., Clinton, J. F., Zenhäusern, G., Ceylan, S., Horleston, A. C., Dahmen, N. L., et al. (2022). S1222a - The largest marsquake detected by insight. *Geophysical Research Letters*, *49*(5), e2022GL101543. https://doi.org/10.1029/2022GL101543

Khan, A., Sossi, P., Liebske, C., Rivoldini, A., & Giardini, D. (2022). Geophysical and cosmochemical evidence for a volatile-rich Mars. *Earth and Planetary Science Letters*, *578*, 117330. https://doi.org/10.1016/j.epsl.2021.117330

Kim, D., Davis, P., Lekić, V., Maguire, R., Compaire, N., Schimmel, M., et al. (2021). Potential pitfalls in the analysis and structural interpretation of seismic data from the Mars InSight mission. *Bulletin of the Seismological Society of America*, *111*(6), 2982–3002. https://doi.org/10.1785/0120210123

Kim, D., Stähler, S. C., Ceylan, S., Lekic, V., Maguire, R., Zenhäusern, G., et al. (2023). Structure along the Martian dichotomy constrained by Rayleigh and love waves and their overtones. *Geophysical Research Letters*, *49*(8), e2022GL101666. https://doi.org/10.1029/2022GL101666

Kobayashi, N., & Nishida, K. (1998). Continuous excitation of planetary free oscillations by atmospheric disturbances. *Nature*, *395*(6700), 357–360. https://doi.org/10.1038/26427

Laske, G., & Widmer-Schnidrig, R. (2015). 1.04 - theory and observations: Normal mode and surface wave observations (pp. 117–167). https://doi.org/10.1016/B978-0-444-53802-4.00003-8

Li, J., Beghein, C., Lognonné, P., McLennan, S. M., Wieczorek, M., Panning, M., et al. (2023). Different martian crustal seismic velocities across the dichotomy boundary from multi-orbiting surface waves. *Geophysical Research Letters*, *50*, e2022GL101243. https://doi.org/10.1029/2022GL101243

Lognonné, P. (2005). Planetary seismology. *Annual Review of Earth and Planetary Sciences*, *33*(1), 571–604. https://doi.org/10.1146/annurev.earth.33.092203.122604

Lognonné, P., Banerdt, W., Clinton, J., Garcia, R., Giardini, D., Knapmeyer-Endrun, B., et al. (2023). Mars seismology. *Annual Review of Earth and Planetary Sciences*, *51*(1). https://doi.org/10.1146/annurev-earth-031621-073318

Lognonné, P., Banerdt, W. B., Giardini, D., Pike, W. T., Christensen, U., Laudet, P., et al. (2019). SEIS: The seismic experiment for internal structure of InSight. *Space Science Reviews*, *215*(1), 12. https://doi.org/10.1007/s11214-018-0574-6

Lognonné, P., Banerdt, W. B., Pike, W. T., Giardini, D., Christensen, U., Garcia, R. F., et al. (2020). Constraints on the shallow elastic and anelastic structure of Mars from InSight seismic data. *Nature Geoscience*, *13*(3), 213–220. https://doi.org/10.1038/s41561-020-0536-y

Lognonné, P., Beyneix, J. G., Banerdt, W. B., Cacho, S., Karczewski, J. F., & Morand, M. (1996). Ultra broadband seismology on. *InterMarsNet. Planet. Space Sci.*, *44*(11), 1237–1249. https://doi.org/10.1016/S0032-0633(96)00083-9

Lognonné, P., & Clévédé, E. (2002). 10 – Normal modes of the Earth and planets. *International Geophysics*, *81*, 125–cp1. https://doi.org/10.1016/S0074-6142(02)80213-3

Lognonné, P., Giardini, D., Banerdt, B., Gagnepain-Beyneix, J., Mocquet, A., Spohn, T., et al. (2000). The netlander very broadband seismometer. *Planetary and Space Science*, *48*(12), 1289–1302. Mars Exploration Program. https://doi.org/10.1016/S0032-0633(00)00110-0

Lognonné, P., & Johnson, C. L. (2015). Planetary seismology. In G. Schubert (Ed.), *Treatise on geophysics* (2nd ed.), (Vol. 10, pp. 65–120). Elsevier. https://doi.org/10.1016/B978-0-444-53802-4.00167-6

Lognonné, P., & Mosser, B. (1993). Planetary seismology. *Surveys in Geophysics*, *14*(3), 239–302. https://doi.org/10.1007/BF00690946

Majstorović, J., Rosat, S., Lambotte, S., & Rogister, Y. (2018). Testing performances of the optimal sequence estimation and autoregressive method in the frequency domain for estimating eigenfrequencies and zonal structure coefficients of low-frequency normal modes. *Geophysical Journal International*, *216*(2), 1157–1176. https://doi.org/10.1093/gji/ggy483

Masters, G., Park, J., & Gilbert, F. (1983). Observations of coupled spheroidal and toroidal modes. *Journal of Geophysical Research*, *88*(B12), 10285–10298. https://doi.org/10.1029/JB088iB12p10285

Nishikawa, Y., Lognonné, P., Kawamura, T., Spiga, A., Stutzmann, E., Schimmel, M., et al. (2019). Mars' background free oscillations. *Space Science Reviews*, *215*(1), 1–26. https://doi.org/10.1007/s11214-019-0579-9

Okal, E. A., & Anderson, D. L. (1978). Theoretical models for Mars and their seismic properties. *Icarus*, *33*(3), 514–528. https://doi.org/10.1016/0019-1035(78)90187-2

Panning, M. P., Banerdt, W. B., Beghein, C., Carrasco, S., Ceylan, S., Clinton, J. F., et al. (2023). Locating the largest event observed on Mars with multi-orbit surface waves. *Geophysical Research Letters*, *50*(1), e2022GL101270. https://doi.org/10.1029/2022gl101270

Panning, M. P., Lognonné, P., Bruce Banerdt, W., Garcia, R., Golombek, M., Kedar, S., et al. (2017). Planned products of the Mars structure service for the insight mission to Mars. *Space Science Reviews*, *211*(1), 611–650. https://doi.org/10.1007/s11214-016-0317-5

Park, J., Lindberg, D. T., & Thomson, D. J. (1987). Multiple-taper spectral analysis of terrestrial free oscillations: Part 1. *Geophysical Journal International*, *91*(3), 755–794. https://doi.org/10.1111/j.1365-246X.1987.tb01668.x

Schimmel, M. (1999). Phase cross-correlations: Design, comparisons, and applications. *Bulletin of the Seismological Society of America*, *89*(5), 1366–1378. https://doi.org/10.1785/bssa0890051366

Schimmel, M., Stutzmann, E., & Ventosa, S. (2018). Low-frequency ambient noise autocorrelations: Waveforms and normal modes. *Seismological Research Letters*, *89*(4), 1488–1496. https://doi.org/10.1785/0220180027

19448007, 2023, 12, Downloaded from https://agupubs.onlinelibrary.wiley.com/doi/10.1029/2023GL103205 by Cochrane France, Wiley Online Library on [07/07/2023]. See the Terms and Conditions (https://onlinelibrary.wiley.com/terms-and-conditions) on Wiley Online Library for rules of use; OA articles are governed by the applicable Creative Commons License

Schimmel, M., Waterhouse, J., Marques, M., & Weinert, D. (2002). Circadian and ultradian rhythmicities in very premature neonates maintained in incubators. *Biological Rhythm Research*, *33*(1), 83–112. https://doi.org/10.1076/brhm.33.1.83.1321

Scholz, J.-R., Widmer-Schnidrig, R., Davis, P., Lognonné, P., Pinot, B., Garcia, R., et al. (2020). Detection, analysis and removal of glitches from insight's seismic data from Mars. *Earth and Space Science*, *7*(11), ESS2681. https://doi.org/10.1029/2020EA001317

Sita, M., & van der Lee, S. (2022). Potential volcano-tectonic origins and faulting mechanisms of three low-frequency marsquakes detected by a single insight seismometer. *Journal of Geophysical Research: Planets*, *127*(10), e2022JE007309. https://doi.org/10.1029/2022JE007309

Smrekar, S. E., Lognonné, P., Spohn, T., Banerdt, W. B., Breuer, D., Christensen, U., et al. (2019). Pre-mission InSights on the interior of Mars. *Space Science Reviews*, *215*(1), 3. https://doi.org/10.1007/s11214-018-0563-9

Stähler, S. C., Khan, A., Lognonné, P., Banerdt, W. B., Giardini, D., Ceylan, S., et al. (2021). Seismic detection of the Martian core. *Science*, *373*(6553), 443–448. https://doi.org/10.1126/science.abi7730

Stutzmann, E., Schimmel, M., Lognonné, P., Horleston, A., Ceylan, S., van Driel, M., et al. (2021). The polarization of ambient noise on Mars. *Journal of Geophysical Research: Planets*, *126*(1), e2020JE006545. https://doi.org/10.1029/2020JE006545

Tanimoto, T., Um, J., Nishida, K., & Kobayashi, N. (1998). Earth's continuous oscillations observed on seismically quiet days. *Geophysical Research Letters*, *25*(10), 1553–1556. https://doi.org/10.1029/98gl01223

Zurn, W., & Rydelek, P. A. (1994). Revisiting the phasor-walkout method for detailed investigation of harmonic signals in time series. *Surveys in Geophysics*, *15*(4), 409–431. https://doi.org/10.1007/bf00666000

19448007, 2023, 12, Downloaded from https://agupubs.onlinelibrary.wiley.com/doi/10.1029/2023GL103205 by Cochrane France, Wiley Online Library on [07/07/2023]. See the Terms and Conditions (https://onlinelibrary.wiley.com/terms-and-conditions) on Wiley Online Library for rules of use; OA articles are governed by the applicable Creative Commons License